Radiology

Thomas K. F. Foo, PhD
David W. Stanley, BS
Ernesto Castillo, MD
Carlos E. Rochitte, MD
Yi Wang, MD
João A. C. Lima, MD
David A. Bluemke, MD, PhD
Katherine C. Wu, MD

Myocardial Viability: Breath-hold 3D MR Imaging of Delayed Hyperenhancement with Variable Sampling in Time[1]

A method for visualizing myocardial infarction with a three-dimensional (3D) breath-hold gated acquisition was examined. By using variable sampling in time, whole heart coverage with a single volume acquisition was achieved in 24 heart beats. In a study of 35 patients, in whom 3D volume acquisition was compared with a two-dimensional (2D) acquisition, all regions of myocardial infarction were correctly identified at 3D examination. The mean imaging time for 12 section locations was 8.0 minutes $\pm$ 3.0 with a 2D approach compared with 22 seconds $\pm$ 4 with a 3D approach ($P < .001$). Advantages were also noted for infarct contrast-to-noise ratio: 60 $\pm$ 37 for 3D versus 33 $\pm$ 20 for 2D imaging ($P < .001$). No significant differences ($P > .05$) were noted at qualitative assessment of myocardial suppression, endocardial border visualization, respiratory and cardiac motion artifacts, or confidence of transmurality of the infarct.

© RSNA, 2004

Delayed hyperenhancement has been shown to indicate nonviable or infarcted myocardial tissue (1–4). Accepted techniques for visualization of nonviable myocardial tissue have used echocardiography-gated fast segmented gradient-recalled echoes preceded by an inversion-recovery preparatory pulse (5). These acquisition techniques generate a two-dimensional (2D) image over 12–16 cardiac cycles (depending on the segmentation and number of signal averages). Complete evaluation (spatial coverage) of the heart in the short-axis (eight to 10 sections) and long-axis (six sections) planes requires 14–16 separate end-expiratory breath holds of 12–16 seconds each. Since rest periods between breath holds are required for patients, a conventional 2D myocardial delayed enhancement examination is usually completed in 8–12 minutes, depending on the ability of the patient to tolerate a fast pace of repeated breath holding.

During this long acquisition period, contrast medium concentration in the myocardium steadily decreases, which leads to varying myocardial T1 relaxation times. Inversion recovery times must then be varied to achieve optimal normal myocardial tissue suppression and contrast enhancement between the first acquisition in the series and the last 2D section imaged (4,6). Moreover, with repeated breath holding, patient fatigue is an increasing issue, especially toward the end of the 2D examination. This leads to the patient being less capable of maintaining a breath hold, and the quality of the images may be degraded at either the apical or basal sections of the heart, depending on the direction of the section prescription.

The purpose of this study was to evaluate a method for visualizing myocardial infarction on magnetic resonance (MR) images by using a three-dimensional (3D) breath-hold gated acquisition.

▮ Materials and Methods

A 3D breath-hold technique for assessing delayed hyperenhancement following the administration of contrast medium was examined. Since whole heart coverage can be achieved within a single

breath hold, the T1 relaxation time of the myocardium is nearly constant during the acquisition of all imaged sections. Thus, a single inversion time can be used for uniform suppression of normal myocardium throughout the imaged volume. Moreover, patients may be able to better tolerate a single, albeit longer, breath hold rather than a repeated series of breath holds.

Acquisition Strategy

To maintain an acquisition time of two heart beats per section partition, a variable asymmetric sampling in time (VAST) scheme was used. This approach is similar to the variable temporal sampling scheme known as block regional interpolation scheme for k space, or BRISK, that was proposed by Doyle et al (7,8). As shown in Figure 1, the central low-spatial-frequency k-space views are interleaved in a common acquisition temporal window of 40 views, with the remaining high-spatial-frequency data acquired sequentially in the second R-R interval. For example, for 192 phase-encoding lines and partial Fourier (0.5 signal average) acquisition, view 96 represents the center of k space, and view 1 represents the highest k-space (spatial frequency) encoded view. In the VAST scheme, views 116, 114, 112, . . . 38, 36 are acquired in one R-R interval for a given section encoding value (40 views). In the next R-R interval, views 115, 113, 111, . . . 37, 35, 34, 33, 32, . . . 3, 2, 1 are acquired (76 views). Note that views 1, . . ., 36 represent the high-spatial-frequency data. To maintain the appropriate phase and magnetization steady state, dummy radiofrequency excitations were included at the end of the first acquisition segment to maintain the same number of radiofrequency excitation pulses applied in each R-R interval.
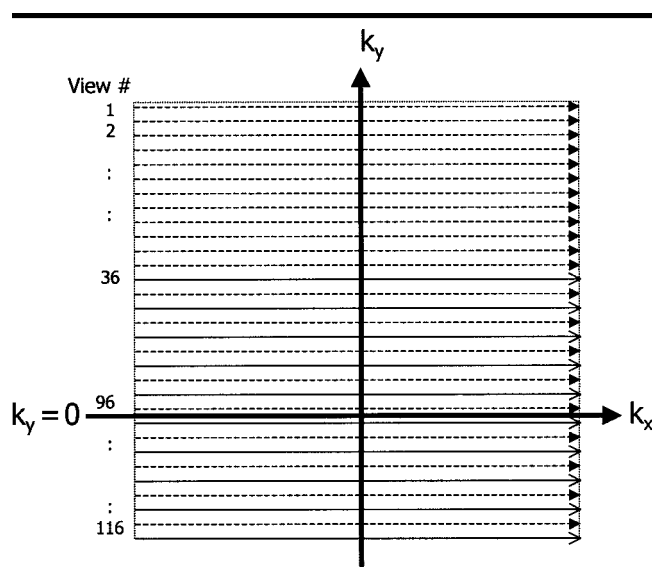
This phase-encoding ordering scheme permits the low-spatial-frequency data to be acquired in a smaller temporal window than does conventional interleaved (time symmetric) ordering. For the given example, VAST acquires the central 80 views within a temporal window of $40 \times$ TR (where TR is the repetition time msec of the sequence), segmented over two R-R intervals. In comparison, symmetric sampling acquires all 116 views within a temporal window ($58 \times$ TR), segmented over two R-R intervals.

In the absence of cardiac motion, VAST and symmetric sampling are equivalent. However, cardiac motion is unavoidable during a 120–240-msec acquisition win-

Figure 1. Graph shows acquisition order for VAST segmentation across two R-R intervals. In this example, 116 total views are acquired in a half-Fourier acquisition. View 96 represents the center of k space and view 1 represents the highest spatial frequency encoded in the phase-encoding (k_y) direction. Views indicated by solid arrows are acquired in one R-R interval, and the remaining views (dashed arrows) are acquired in the next R-R interval for each partition-encoding step.

Figure 2. Graph shows point spread function of object moving to the right at a velocity of 40 mm/sec for VAST segmentation and symmetric segmentation. Note that the primary peak is narrower for VAST segmentation, but a secondary lower-amplitude peak (displaced from the primary peak) is also generated.
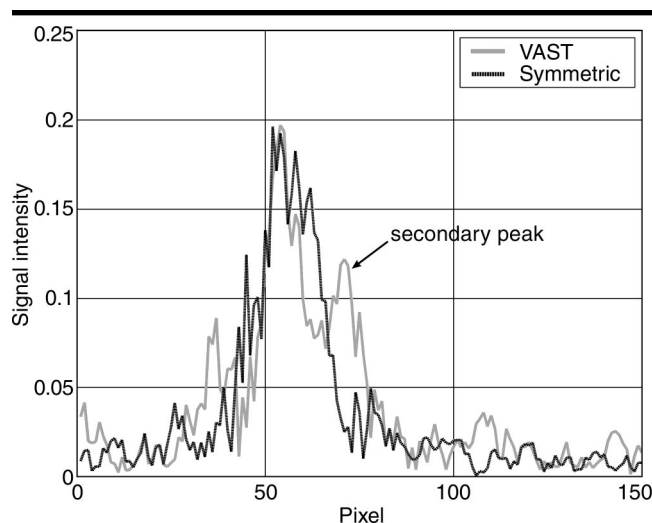
dow. For constant linear motion of a point object throughout the temporal acquisition window, VAST achieves a sharper point spread function than does symmetric sampling (as shown in Fig 2), but it also generates a low-amplitude ghost artifact distal to the primary edge.

In the presence of motion during the acquisition window, each phase-encoding view registers a phase shift equivalent to the displacement of the target object at the time of data acquisition. In image space, this phase shift produces a displacement of the component of the target object proportional to the spatial frequency content of the object. The higher the spatial frequency, the lower the signal intensity of the ghost or motion artifacts.

By grouping the high spatial frequencies into a single acquisition window, motion or ghost artifacts are displaced further from the original position of the target object. The result is a smaller point spread function than can be obtained if the phase-encoding views were segmented equally in each R-R interval.

The optimal acquisition scheme is to acquire all relevant data in the smallest possible temporal window. This can be achieved through trade-offs between temporal resolution and spatial coverage; greater segmentation results in either increasing the breath-hold period or decreasing the number of partitions (for the same breath-hold time). VAST segmentation permits a smaller degree of segmentation while preserving the point spread function of a smaller temporal window.

Pilot Study: Determination of Optimal Segmentation Order

Prior to the primary study, in which 2D and 3D delayed hyperenhancement acquisitions were compared, a preliminary pilot study was conducted to determine the appropriate segmentation order. This study consisted of a blinded evaluation in five patients (four men, one woman; mean age, 59 years ± 11; mean weight, 71 kg ± 12) with the use of both symmetric and VAST segmentation of k space. The patients had possible myocardial infarction and were referred for cardiac MR imaging. Informed consent was obtained, as well as approval from the local institutional ethics board (institutional review board). The images were scored by a cardiologist (C.E.R., 10 years experience), who graded image quality and edge sharpness by visual inspection.

In the initial evaluation of k-space sampling order, better edge definition and fewer artifacts were noted in the MR images obtained with VAST. Among the five patients examined in the pilot study, image quality was equivalent (between VAST and the conventional temporally symmetric sampling) in three patients and better with VAST in two patients. On the basis of these results, the subsequent 3D volume evaluations were conducted with VAST. In the evaluation of the pilot study MR images, subtle differences were identified by the observers (C.E.R., T.K.F.F., D.W.S.), especially in the definition of the infarcted zone and of the myocardial boundaries.

Experimental Protocol

All examinations were conducted with a 1.5-T cardiac MR imager (Signa CV/i;

GE Medical Systems, Waukesha, Wis) with high performance gradients (40 mT/m, 150 T/m/sec). A fast 3D gradient-recalled echo pulse sequence was modified to allow inversion-recovery prepared segmented electrocardiography-gated acquisitions. A four-element cardiac phased-array coil was also used. In all evaluations, images were obtained in mid-to-end systole. To provide a uniform comparison for the 2D and 3D MR images in the same patient, the same inversion time (200–250 msec) was used in all delayed enhancement imaging in the same patient. An initial inversion time of 200 msec was used. If the remote (normal) myocardial signal suppression was not sufficient, single-section 2D MR imaging was repeated with a different inversion time. The inversion time (determined to provide optimal suppression) was then used for all subsequent imaging. Different inversion times were used in different patients to account for the variability in contrast media uptake in the myocardium between patients. However, once the inversion time for each patient was determined, the same inversion time was used for both the 2D and 3D delayed enhancement MR imaging examinations.

The imaging parameters for the 2D acquisition were 5.4–7.1/1.4–3.2 (repetition time msec/echo time msec), 256 × 160 to 256 × 192 acquisition matrix, 24 views per segment, two signal averages acquired, 20° flip angle, an imaging time of 12–14 heart beats per section location, and 12–14 contiguous sections of 8.0 mm each. In comparison, the 3D parameters were similar except for the following: 3.3–4.3/1.5–1.9, 256 × 160 acquisition matrix, 0.5 signal average acquired, 12 partitions of 8.0 mm, and an imaging time of 24 heart beats. Partial-phase field of view between 0.75 and 1.0 was also used, depending on patient size.

In the primary study, 35 patients (29 men, six women; mean age, 58 years ± 10) were enrolled according to local institutional review/ethics board–approved protocols with informed consent. Of the 35 patients, seven were considered negative for myocardial infarction, as they had negative results at (x-ray) angiography and normal enzyme levels ($n = 1$); negative results at nuclear medicine imaging and normal enzyme levels ($n = 1$); negative results at angiography only ($n = 1$); negative results at nuclear medicine imaging only ($n = 1$); negative results at angiography but elevated enzyme levels ($n = 1$); mild 20% stenosis at angiography but normal enzyme levels ($n = 1$); or normal enzyme levels and sarcoidosis ($n = 1$).

In the patient examinations, 2D myocardial delayed enhancement MR images were acquired approximately 10–15 minutes after a cumulative dose of 0.2 mmol extracellular gadolinium-based contrast medium per kilogram of patient weight was administered. Immediately after the 2D MR imaging examination, the 3D breath-hold MR imaging examination was performed. The 3D myocardial delayed enhancement MR images were acquired 16–27 minutes after the contrast medium administration. Imaging time for all sections in the 2D and 3D examinations was measured as part of the comparison. The 2D and 3D images were not alternated because of the time needed to complete acquisition of the 2D MR images.

Images from the 2D series and the 3D volume were prepared electronically for each patient studied and were presented to three clinical reviewers (two radiologists [D.A.B., 9 years experience; E.C., 4 years experience] and a cardiologist [K.C.W., 5 years experience]) working independently. Each blinded reader was asked to evaluate the images by using a five-point scale (scale of 0–4) in the following categories: degree of myocardial suppression, visualization of endocardial borders, respiratory motion artifacts, cardiac motion artifacts, and confidence of transmurality. The qualitative categories were defined as follows: unacceptable or poor quality (score of 0); artifacts present, not diagnostic (score of 1); acceptable with some artifacts, borderline diagnostic (score of 2); good quality, minimal artifacts, diagnostic (score of 3); or excellent quality, no artifacts, diagnostic (score of 4). Scores of 3 and higher were deemed as acceptable for diagnostic purposes. Note that for confidence of transmurality, the categories were defined as follows: unable to discern transmurality/poor image quality (score of 0); artifacts present, no confidence (score of 1); acceptable image quality, marginal confidence (score of 2); good image quality, high confidence (score of 3); or excellent image quality, very high confidence (score of 4). There was no consensus reading or collective interpretation of the data.

Image contrast (signal difference–to-noise ratio = $[A - B]/\sigma$, where A and B are signal intensities in the infarcted and normal [remote] myocardial regions, respectively, and σ is the SD in a region of background noise—an area in the image with an absence of signal), was also measured in each instance in patients with an identifiable myocardial infarction. A small circular region of interest (100–140

mm^2) was placed in the infarcted area in approximately the same location in both the corresponding 2D and 3D MR images. The adjacent remote (normal) myocardial tissue signal intensity was also measured in the same way. The regions of interest were placed by a scientist (D.W.S.) working independently of the three blinded clinical reviewers. The signal difference–to-noise ratio was used as a measure of contrast to provide a display-independent metric (10).

Statistical Analysis

The qualitative scores assigned by each reviewer were averaged for each patient and for each technique (2D and 3D). Analysis of paired t tests (two sample means) was performed on the results to assess the statistical significance of the scores. $P < .05$ was considered to denote statistical significance. The procedure used was as follows: For each measurement or assessment category, the scores for each patient were averaged for all three reviewers to compute separate average scores for the 2D and 3D examinations. Analysis of paired t tests (two sample means) was performed on the results to assess the statistical significance of the different scores assigned to the 2D and 3D MR images in all 35 patients.

❚ Results

The Table shows mean scores of the qualitative image assessment among all observers and includes the quantitative measurements of imaging time and lesion contrast enhancement. Of the patients examined, seven did not have a myocardial infarct (determined from negative results at 2D delayed enhancement MR imaging and results of prior clinical examinations). The same seven patients were those who did not have clinical evidence of myocardial infarction. All seven were correctly identified as having no evidence of myocardial infarction at both the 2D and 3D MR image set assessments. In all categories, except for the categories of image contrast and cardiac motion artifacts, there were no statistical differences in image quality between 2D and 3D MR images ($P > .05$).

The 3D images had signal difference–to-noise ratios that were improved by a factor of 2 (59.8 ± 37.2) compared with the 2D images (32.8 ± 19.7) ($P < .001$). The acquisition window was 130–170 msec for 2D imaging compared with 110/220 msec (low/high k space) for the 3D myocardial delayed enhancement imag-

Mean Observer Scores and Measurements for 2D and 3D MR Images

| Evaluation Parameter	2D Imaging	3D Imaging	P Value
Quantitative			
Signal difference–to-noise ratio	32.8 ± 19.7	59.8 ± 37.2	<.001
Imaging time	14 heart beats	24 heart beats	NS
Total imaging time for 12 sections (sec) ($n = 29$)	481 ± 179	22 ± 4	<.001
Qualitative			
Myocardial suppression	3.5 ± 0.7	3.4 ± 0.5	NS
Endocardial border visualization	3.1 ± 0.8	3.1 ± 0.6	NS
Respiratory motion artifacts	3.7 ± 0.5	3.5 ± 0.7	NS
Cardiac motion artifacts	3.6 ± 0.4	3.5 ± 0.3	NS
Confidence of transmurality	3.6 ± 0.7	3.6 ± 0.4	NS

Note.—Qualitative data are means (±SD) of scores assigned by three blinded readers, scored on a scale of 0–4; scores of 3 and above are good or excellent. NS = not significant.
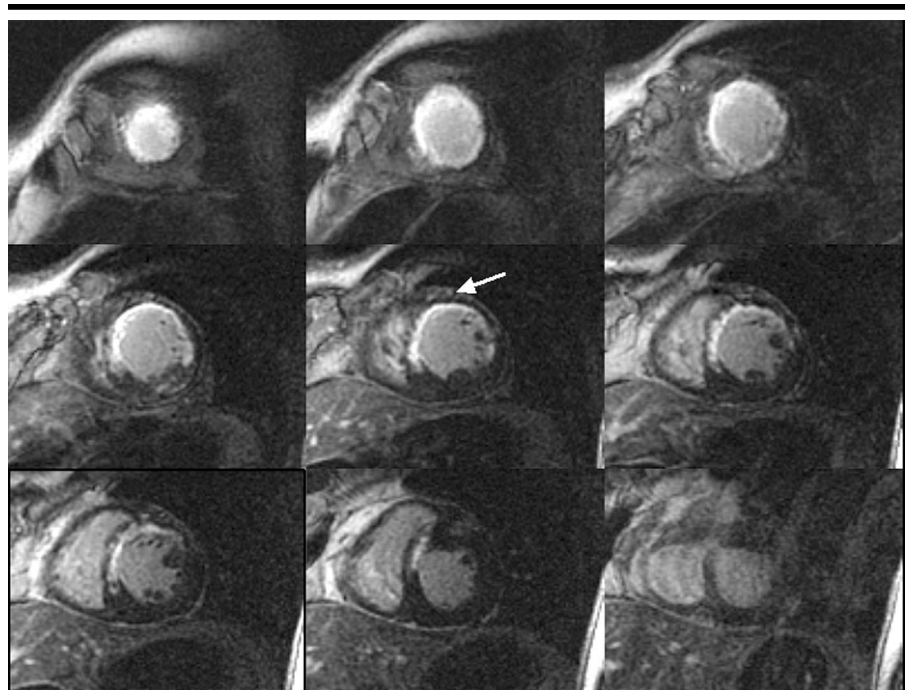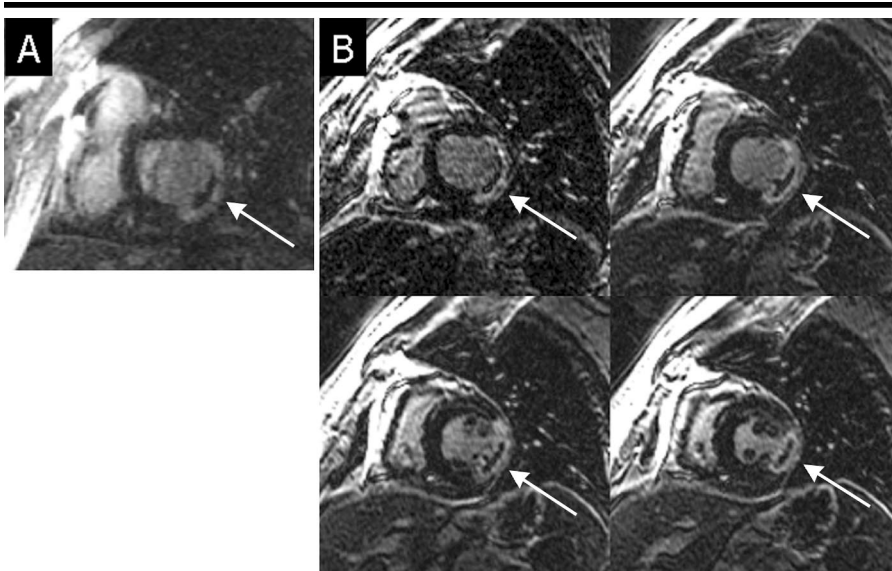

Figure 3. Breath-hold 2D short-axis MR images acquired in a 54-year-old man with an anterior-septal infarct (arrow). Each image was acquired with a separate 11-second breath hold. Total acquisition time for all nine section locations was 6.3 minutes. Note that as fatigue set in, the patient's ability to maintain a breath hold deteriorated, leading to respiratory motion artifacts noted in the last breath-hold image of the series (bottom right image). Acquisition parameters were 36 × 27-cm field of view, nine sections of 8.0 mm, 7.2/3.2, 20° flip angle, ± 31.25-kHz receiver bandwidth, 256 × 192 matrix, and two signals acquired.

ing, which contributed to a slightly better mean score for cardiac motion artifacts in the 2D imaging examinations (not statistically significant). A 2D MR acquisition obtained in a patient with a chronic anterior septal infarct is shown in Figure 3. Among the nine section locations in this series, respiratory motion artifacts were noted at the last breath-hold acquisition because of patient fatigue. Comparable overall image quality was observed in the corresponding 3D acquisition (Fig 4).

In five of 35 patients, it was obvious that the later images acquired in the 2D examination contained increased respiratory artifacts due to increasing patient fatigue (Figs 3, 5). However, this was an observation of the entire 2D image set, and no statistical evaluation was performed. Motion artifacts were considered to be present in the 2D data set if the severity was similar to that noted in Figures 3 and 5. In the example shown in Figure 5, respiratory motion artifacts were noted in the 2D image, and the
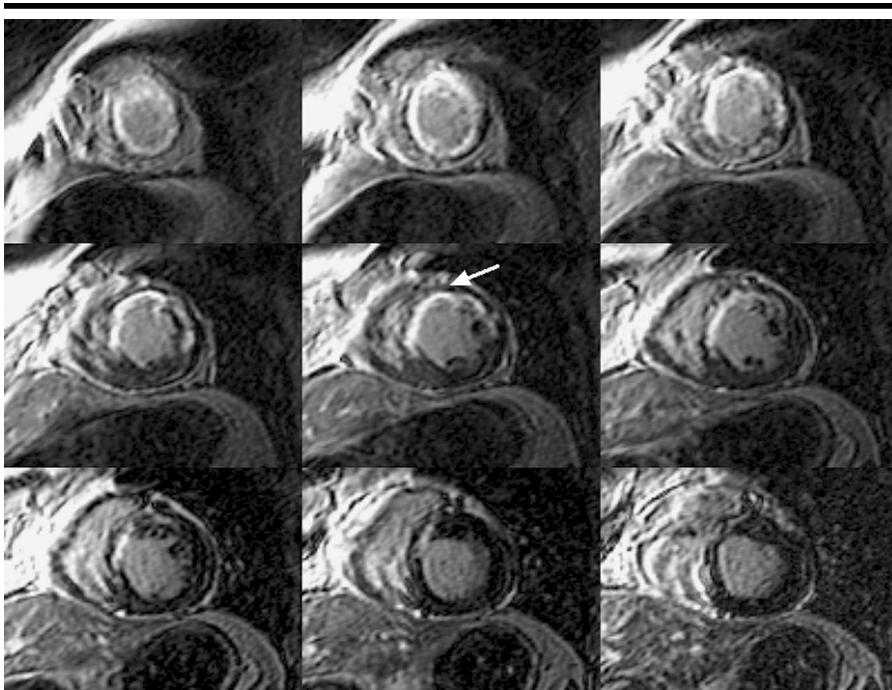
Figure 4. Breath-hold 3D short-axis MR images acquired in same patient as in Figure 3. Images from 12 contiguous locations were acquired in a single 19-second breath hold. Comparable definition of the infarcted zone (arrow) was noted in the 3D image. However, a single breath hold was sufficient to acquire images covering the whole heart. Acquisition parameters were 36 × 29-cm field of view, 12 partitions of 8.0 mm interpolated to 4.0 mm partitions, 3.8/1.4, 20° flip angle, ± 62.5-kHz receiver bandwidth, 256 × 160 matrix, and 0.5 signal acquired. Overall image quality rating for this data set (averaged among three readers) was 3.0, compared with 3.3 for the corresponding 2D data set. Lesion contrast (signal difference–to-noise ratio) was 106.2 versus 62.3 for the 2D measurements in Figure 3.

Figure 5. Breath-hold short-axis MR images in a 59-year-old patient with an inferior wall infarct (arrow) corresponding to a left circumflex artery lesion. *A*, In this 2D image, fourth acquisition in a series of 9-second breath holds, patient fatigue contributed to a nonoptimal breath hold, resulting in respiratory motion artifacts and overall degradation of image quality. *B*, 3D images (only four partitions of 12 noninterpolated partitions shown) were acquired in 17 seconds. The hyperintense infarcted zone (arrow) is clearly visible with the central hypointense zone, indicative of microvascular obstruction. Acquisition parameters were 38 × 34-cm field of view, 12 partitions of 8.0 mm, 3.8/1.4, 20° flip angle, ± 62.5-kHz receiver bandwidth, 256 × 160 matrix, and 0.5 signal acquired.

extent of the myocardial infarction (including the no-reflow zone, indicative of microvascular obstruction [9]) was better delineated in the 3D image.

Although the mean breath-hold time for 2D imaging was 12 seconds, compared with 22 seconds for 3D imaging, rest periods in between breath holds extended the overall time per section to almost 40 seconds (for a total of 480 seconds to acquire 12 sections). The 3D technique reduced the overall imaging time for a myocardial delayed hyperenhancement examination by a mean of 8 minutes among all patients studied.

Image Artifacts

Although there were no significant differences between the techniques in the ability to depict myocardial infarction in the patient population evaluated, there were differences in the appearance of the 3D images compared with the 2D images. The 3D images had a more speckled appearance in the myocardium that may make it more difficult to evaluate for diffuse fibrosis, such as in hypertrophic cardiomyopathy or muscular dystrophy. The 3D images had an overall lower mean noise floor than did the 2D images. The mean noise floor for the 3D images was 2.1 ± 0.2, while that for the 2D images was 4.6 ± 1.3. A paired t test (two sample means) provided a P value that indicated that this observation was statistically significant ($P < .001$). The lower mean noise floor permitted smaller variations in signal intensity to be more easily observable in the 3D images than in 2D images. As shown in Figure 6, the mean signal intensity in the background (noise floor) was a factor of 2 lower in the 3D image than in the 2D image. Even though the inferior wall infarct was well delineated in both images, signal intensity variations in the normal (remote) myocardium were more prominent in the 3D images than in the 2D images.

Another possible artifact with the breath-hold 3D acquisition is caused by the longer acquisition window during which magnetization may vary substantially, especially if the T1 relaxation is very short. This leads to a ghost artifact, which may be confused with a subendocardial infarct (Fig 7). This artifact can be easily identified, as it disappears on switching the frequency and phase-encoding direction. Note that this artifact can also be observed in a 2D acquisition sequence when the acquisition window is of comparable duration to that in the

3D acquisition. However, this ghost artifact is more obvious in the 3D images because of the lower noise floor of the 3D acquisitions.

Discussion

The VAST approach was determined to provide equivalent ability to identify the infarcted regions in all cases. Overall, the signal difference–to-noise ratio was superior than that in the 2D images. The ability to acquire an entire 3D volume in such a short time also permits the use of respiratory navigator gating (11) with substantially reduced imaging time (12). If we assume a conservative 30% imaging efficiency, a free-breathing 3D examination with 12 partitions can be completed in about 80 heart beats (80 seconds, assuming a heart rate of 60 beats per minute). With such short free-breathing imaging times, fast navigators provide the opportunity to either increase the segmentation (to reduce the temporal acquisition window) or increase the number of partitions, with reduced partition thickness.

The ability to rapidly acquire images from a 3D volume in a single breath hold was achieved without the use of parallel imaging techniques (13–15). The proposed 3D technique is compatible with parallel imaging. Hence, the overall imaging time can be reduced by a factor of 2 or more. This reduction in imaging time can also be traded-off to improve temporal and spatial resolution. As a disclaimer, there were no surgical clips or stents in any of the patients we studied, and none had undergone any other interventional procedure that would increase the probability of image artifacts due to increased magnetic susceptibility (caused by the presence of metallic objects). However, since the primary acquisition sequence was a gradient-recalled-echo sequence with a short echo time, magnetic susceptibility artifacts from surgically implanted metallic objects are not anticipated to pose a major problem.

Image artifacts from the 3D acquisition (as described previously) were relatively subtle and did not adversely affect the qualitative analysis. However, the patient population studied did not include patients with small diffuse regions of enhancement. To avoid misinterpretation from these circumstances, a confirmatory targeted 2D acquisition could be performed at one or two spatial locations. This confirmatory acquisition could be of higher spatial resolution to better evalu-

Figure 6. Short-axis breath-hold MR images in a 65-year-old man with an inferior wall infarct. Both the 3D *(A)* and 2D *(B)* approaches delineated the infarcted zone. However, because of the decreased mean background signal intensity in the 3D image (2.5 ± 0.8), small signal intensity variations (arrows) were more apparent in the 3D image than in the 2D image (5.1 ± 1.3) with the lower noise floor. Note that the endocardial borders of the infarct could be better distinguished from the ventricular blood pool with the 3D acquisition.
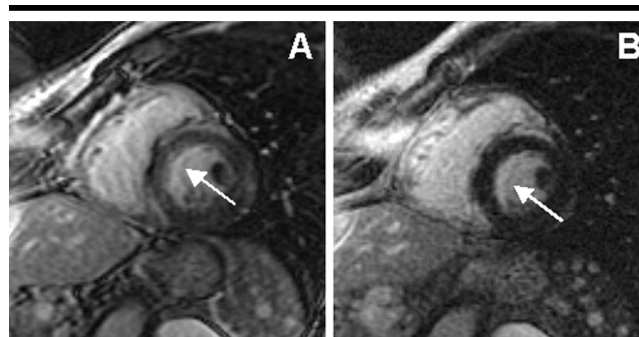
Figure 7. Breath-hold short-axis MR images in a 43-year-old patient obtained with the 3D *(A)* and 2D *(B)* approach. An area of apparent hyperintensity was noted near the septal wall, indicating a possible subendocardial infarct. On closer inspection, this artifact (arrow) was noted to be in the left ventricle rather than in the septal myocardial tissue. This case was correctly assessed as negative for myocardial infarct. The 2D image also shows a similar artifact that was less apparent because of a higher noise floor. Note that the signal intensity of the artifact is much lower than that encountered in a case of true hyperenhancement.
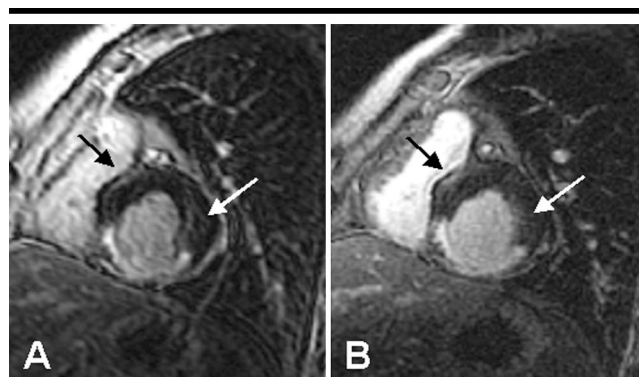
ate small isolated regions of diffuse fibrosis in patients with hypertrophic cardiomyopathy or muscular dystrophy.

Since images at all section locations were acquired in a single breath hold, there is no need to have precise reproduction of the breath-hold position, and thus a choice of end-inspiration or end-expiration breath hold is allowed. Under some circumstances, the patients were unable to maintain an effective end-expiration breath hold. In such cases, end-inspiration breath holds were successfully used. Since the 3D acquisition is a single breath-hold acquisition, the poor reproducibility of the end-inspiration breath-point positions was not an issue.

Unlike 2D acquisitions, in which sections from different end-inspiration breath holds are misregistered, all partitions from a 3D volume acquisition are inherently registered.

Another advantage of a 3D volume acquisition technique is that there is less inflow enhancement effect in the ventricular blood pool. This enabled the endocardial boundaries of the infarcted zone to be better defined than in the 2D images. Lesion contrast enhancement was also significantly better ($P < .001$) for the 3D acquisition, with significantly shorter imaging times.

In conclusion, in all examinations, we were able to use a single 3D breath-hold

acquisition to achieve whole heart coverage, with image quality equivalent to that of a multiplanar multiple breath-hold 2D acquisition. Overall, by using the 3D approach, the examination time for a myocardial viability study can be reduced to a single breath hold. The fast acquisition allows for repeated acquisitions at different inversion times for global T1 measurements of the whole heart without correcting for changes in contrast medium concentration, as is encountered with whole heart 2D imaging. Moreover, the 3D approach can be used in an end-inspiration breath-hold acquisition, since there is no need to obtain multiple reproducible (end-expiratory) breath-hold positions as there is in 2D examinations. This improves patient tolerance and reduces patient fatigue. We have demonstrated that the 3D VAST myocardial delayed enhancement approach is robust and time efficient. Equivalent diagnostic information was obtained with the proposed 3D approach for myocardial delayed enhancement MR imaging compared with the conventional 2D acquisition techniques, at a substantial reduction in overall imaging times.

References

1. Lima JA, Judd RM, Bazille A, Schulman SP, Atalar E, Zerhouni EA. Regional heterogeneity of human myocardial infarcts demonstrated by contrast-enhanced MRI: potential mechanisms. Circulation 1995; 92:1117–1125.
2. Wu KC, Kim RJ, Bluemke DA, et al. Quantification and time course of microvascular obstruction by contrast-enhanced echocardiography and magnetic resonance imaging following acute myocardial infarction and reperfusion. J Am Coll Cardiol 1998; 32:1756–1764.
3. Wu KC, Zerhouni EA, Judd RM, et al. Prognostic significance of microvascular obstruction by magnetic resonance imaging in patients with acute myocardial infarction. Circulation 1998; 97:765–772.
4. Kim RJ, Fieno DS, Parrish TB, et al. Relationship of MRI delayed contrast enhancement to irreversible injury, infarct age, and contractile function. Circulation 1999; 100:1992–2002.
5. Simonetti OP, Kim RJ, Fieno DS, et al. An improved MR imaging technique for the visualization of myocardial infarction. Radiology 2001; 218:215–223.
6. Kim RJ, Wu E, Rafael A, et al. The use of contrast-enhanced magnetic resonance imaging to identify reversible myocardial dysfunction. N Engl J Med 2000; 343:1445–1453.
7. Doyle M, Walsh EG, Blackwell GG, Pohost GM. Block regional interpolation scheme for k-space (BRISK): a rapid cardiac imaging technique. Magn Reson Med 1995; 33:163–170.
8. Doyle M, Walsh EG, Foster RE, Pohost GM. Rapid cardiac imaging with turbo BRISK. Magn Reson Med 1997; 37:410–417.
9. Rochitte CE, Lima JA, Bluemke DA, et al. Magnitude and time course of microvascular obstruction and tissue injury after acute myocardial infarction. Circulation 1998; 98:1006–1014.
10. Wolff SD, Balaban RS. Assessing contrast on MR images. Radiology 1997; 202:25–29.
11. Ehman RL, Felmlee JP. Adaptive technique for high-definition MR imaging of moving structures. Radiology 1989; 173: 255–263.
12. Saranathan M, Rochitte CE, Hoppel BE, Foo TK. Fast three-dimensional, free-breathing imaging of myocardial infarction (abstr). In: Proceedings of the 10th Meeting of the International Society for Magnetic Resonance Imaging in Medicine. Berkeley, Calif: International Society for Magnetic Resonance in Medicine, 2002; 1623.
13. Sodickson DK, Manning WJ. Simultaneous acquisition of spatial harmonics (SMASH): fast imaging with radiofrequency coil arrays. Magn Reson Med 1997; 38:591–603.
14. Pruessmann KP, Weiger M, Scheidegger MB, Boesiger P. SENSE: sensitivity encoding for fast MRI. Magn Reson Med 1999; 42:952–962.
15. Sodickson DK. Tailored SMASH image reconstructions for robust in vivo parallel MR imaging. Magn Reson Med 2000; 44: 243–251.